Available online at www.CivileJournal.org

# Civil Engineering Journal

(E-ISSN: 2476-3055; ISSN: 2676-6957)

Vol. 11, No. 03, March, 2025

# Cluster-Driven Predictive Model for Asphalt Pavement Maximum Temperature in Tropical Airport

Pebri Herry [1*], Ade Sjafruddin [1], Bambang S. Subagio [1], Eri S. Hariyadi [1]

[1] *Department of Civil Engineering, Faculty of Civil Engineering and Environment, Bandung Institute of Technology, Bandung, Indonesia.*

Received 05 December 2024; Revised 27 January 2025; Accepted 11 February 2025; Published 01 March 2025

**Abstract**

The majority of runways are constructed using flexible pavement surfaced with Hot Mix Asphalt (HMA). The performance of these materials is significantly influenced by temperature due to their viscoelastic nature. Understanding the maximum temperature profile in the HMA layer is essential for evaluating pavement load-bearing capacity and durability. Therefore, this study aimed to present a robust model for predicting maximum pavement temperature distributions based on direct measurements from 13 strategically selected airports in the tropical region of Indonesia. Data was collected using the Airside Pavement Sensing System (AirPaSS), a monitoring device that integrated solar-powered energy management, automated data transmission, and multi-depth thermocouple sensors, providing real-time and accurate temperature measurements. By using hierarchical clustering, airports were categorized into three clusters based on air temperature, pavement temperature, and elevation, enabling precise and cluster-specific material design. The result showed that the predictive model incorporating linear and logarithmic regression achieved high accuracy, with Root Mean Squared Error (RMSE) values ranging from 0.91°C to 2.01°C and Adjusted $R^2$ values between 0.76-0.91. This model offered a practical solution for predicting HMA layer temperature at any depth. The results provided valuable information for performance-based grading systems with significant implications for improving infrastructure resilience in tropical and similar climatic regions.

*Keywords:* Airport Pavement; Pavement Temperature; Temperature Prediction Model; AirPaSS.

## 1. Introduction

The service life of flexible pavement surfaced with Hot Mix Asphalt (HMA) is susceptible to gradual degradation because of the interplay between traffic loads and constant direct exposure to environmental loads [1]. The strength of HMA as a viscoelastic material is greatly influenced by moisture and temperature variations. Moisture and temperature significantly affect pavement structure performance, with long-term effects observed on the response to loads. According to Sulejmani et al. [2], experiments have shown that temperature and humidity substantially contribute to strains in HMA mixtures. Temperature is the dominant factor determining the performance of the HMA mixture [3-6], with the stress-distributing ability decreasing significantly as temperature rises. Therefore, predicting temperature distribution in HMA layers is essential to understand flexible pavement strength characteristics.

Despite the distinct climate conditions of tropical regions, comprehensive studies on pavement temperature characteristics are very limited. Flexible pavements in tropical regions are more susceptible to rutting, as shown by the visual assessments by Wibowo et al. [7]. This shows the need for a comprehensive study to predict temperature distribution characteristics of HMA in tropical regions. The pavement temperature prediction model is applied in the design and evaluation, aging assessment, as well as asphalt grading selection using the Performance Grading (PG) system during mix design [8].

* Corresponding author: 35021306@mahasiswa.itb.ac.id

http://dx.doi.org/10.28991/CEJ-2025-011-03-01

During the design and evaluation of flexible pavement, most guidelines depend on a single design temperature. For example, in tropical countries such as Indonesia, design guidelines typically specify a weighted mean annual pavement temperature (WMAPT) of 38°C for mountainous areas and 41°C for coastal regions [9]. However, using a single value for design temperature can introduce errors due to inaccurate indication of local temperature variations. A more reliable method will include using a robust temperature prediction model capable of providing accurate and site-specific pavement temperature for design purposes. Regarding PG binder grading selection, prediction models aided in providing the required information on the representative high (PG 58 to 82) and low (PG -10 to -40) ranges of temperature. For grading selection, prediction of low temperature is also useful for cold regions, where a pavement temperature prediction model is used to develop strategies to prevent icing [10].

Based on the background, this study aimed to propose an asphalt pavement maximum temperature prediction model using comprehensive direct field measurement of airports in the tropical region of Indonesia. This country is currently operating approximately 301 airports, and all runways are constructed using flexible pavement surfaced with HMA mixtures [11]. In tropical regions, there is no urgent need for a minimum temperature prediction model since pavement temperature is not below 0°C. Initially, this study started with the importance of a pavement temperature prediction model for construction purposes, followed by a comprehensive review and discussion of previous related investigations, identifying key gaps in the field. The method used was fully discussed, including the process for selecting data reading locations. Subsequently, an in-depth explanation of the Airside Pavement Sensing System (AirPaSS) was provided, emphasizing reliability and accuracy. The model development process was also carried out, discussing the selection of parameters and clustering of pavement temperature data across the Indonesian tropical archipelago. Finally, this study provided insights into model performance by comparing predicted and recorded data.

## 2. Review of Pavement Temperature Prediction Model

Several studies have been conducted to predict pavement temperature, with models developed based on three main methods, namely numerical or Finite Element Models (FEM), theoretical or analytical, as well as statistical and probabilities [12, 13]. Numerical methods are less user-friendly due to the need for proficiency in formulating FEM and exercising sound judgment to ensure solution convergence [13, 14]. Analytical methods focus on temperature prediction for multilayer asphalt pavement, encountering complexity in deriving a closed-form solution [13, 15, 16]. Ayasrah et al. [17] proposed an analytical model to predict the surface temperature of flexible pavements, accounting for environmental factors, such as air temperature and solar flux, especially in arid regions. This model helps assess temperature variations, which are essential for understanding and modeling thermal cracking in pavements. The latest development starts implementing artificial intelligence in the development of HMA temperature prediction models [18, 19]. Among all methods, statistical analysis was the most used and developed despite requiring a large number of datasets [13]. Several models have been statistically developed using local climate data from various regions globally, including the United States [20], China [21], Oman [22], Yemen [23], Saudi Arabia [24], Iran [25], Libya [26], India [27], Indonesia [28], and Ghana [29].

The previous model developed for tropical climates in Indonesia [28] was practical and straightforward, but the applicability was confined to certain depths. This development was based on 10-day data obtained during the dry season at intervals of 30 minutes, excluding model coverage during the wet season. Additionally, the model had not been validated for use in other locations. Another model was developed for the tropical region in Ghana [29] based on temperature observation at two locations, which was recorded at the surface and mid-depth of HMA. Although accurate results were obtained, further studies were recommended to improve the proposed models, including data collected at additional locations and over a longer duration.

The most recent pavement temperature prediction model for the tropical region of Indonesia has been introduced by Herry et al. [30]. This model was developed using direct temperature measurements from pavement at Komodo International Airport and validated for application in another region. Based on Herry et al. [30], the model showed the next step in advancing pavement temperature prediction in Indonesia. Therefore, this study introduced a new model, developed using a more extensive dataset of direct pavement temperature measurements from 13 airports, strategically selected to represent the diverse geographical and climatic conditions across the Indonesian tropical region. By expanding the scope of data collection, analysis was conducted to enhance the model's robustness and applicability, providing a more comprehensive tool for pavement temperature prediction in tropical regions.

## 3. Problem Statement and Objectives

The performance of flexible pavement is significantly influenced by temperature variations, which affect the stiffness of asphalt mixtures and alter the stress distribution in pavement structure. At high temperatures, asphalt stiffness decreases, increasing the risk of permanent deformation, such as rutting, and causing excessive stress transfer to underlying layers, leading to structural distortions. Conversely, asphalt mixtures at low temperatures are brittle, showing susceptibility to thermal cracking. These temperature-induced characteristics underscore the need for accurate temperature prediction models focused on specific climatic conditions, ensuring optimal pavement performance.

A comprehensive understanding of temperature characteristics and their distribution across asphalt layer cross-section, as observed in the field, is essential for designing effective pavements. Identifying the maximum and minimum pavement temperatures is also important, as accurate temperature profiles inform the selection of suitable materials and provide insights into potential damage mechanisms. This knowledge forms the foundation for developing efficient repair strategies and ensuring the long-term durability as well as performance of pavement systems.

Existing pavement temperature prediction models are often developed based on localized data, limiting their applicability. In Indonesia, available models are overly simplistic and have not been validated for diverse climatic regions or conditions beyond the data used in their development. In the aviation sector, many airports still depend on penetration-system specifications, which are less effective in addressing temperature variability compared to PG systems. Therefore, a comprehensive understanding of temperature effects is essential for the broader adoption of performance-based specifications, improving the resilience of airport pavements under Indonesia's unique climatic conditions.

This study aimed to establish a comprehensive framework for predicting pavement temperature distribution across Indonesian airports by clustering into several distinct groups based on climatic and geographical conditions. Leveraging a novel real-time monitoring device equipped with advanced thermocouple sensors, solar-powered energy management, and automated data transmission, this study enhanced dataset reliability and provided deeper insights into thermal behavior across various pavement layers. Subsequently, an analysis was carried out to develop and validate a predictive model for maximum pavement temperature at various depths of asphalt mix pavements at airports to achieve high accuracy and reliability. By integrating the temperature prediction model with airport cluster classifications, the results provided supporting data to the optimization of pavement design, ensuring enhanced performance and durability under diverse environmental conditions.

## 4. Research Methodology

This study focused on the systematic collection of pavement temperature data from airports located across Indonesia's main islands, capturing diverse climatic and geographical conditions. Temperature readings were recorded over 300–500 days at 15-minute intervals to obtain a robust dataset for analysis. This comprehensive dataset was used to identify pavement temperature clusters, forming the basis for developing classifications of specific environmental conditions, with the method shown in Figure 1.

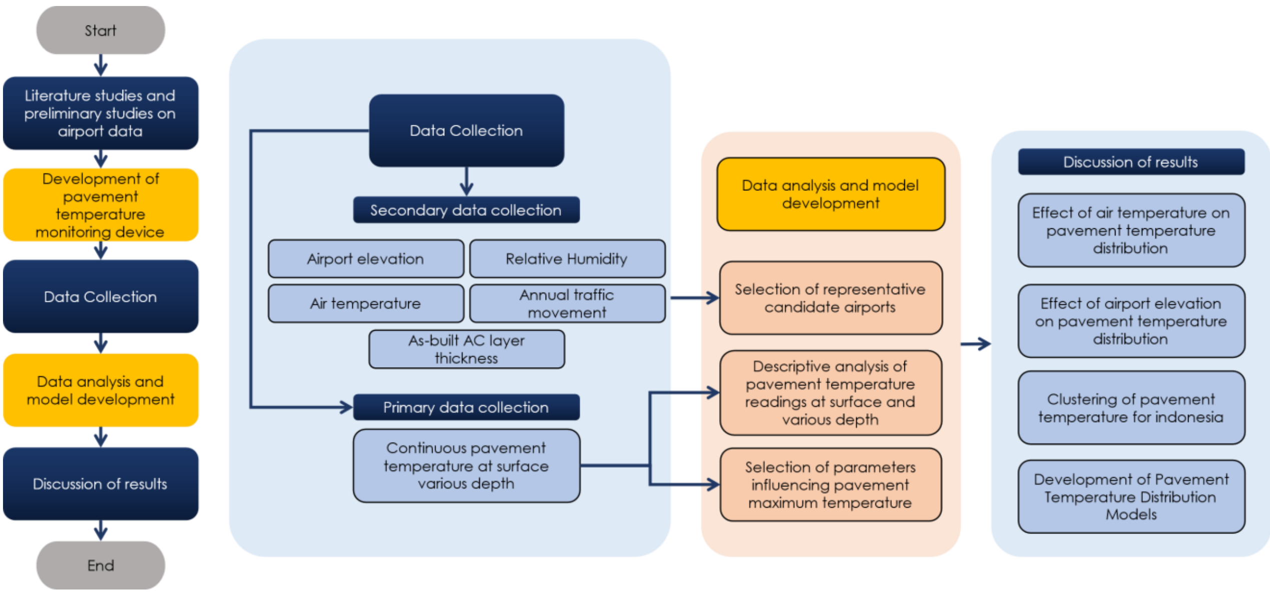


**Figure 1. Flowchart of the research methodology**

## 5. Selection of Candidate Airport for Pavement Temperature Monitoring

This study was carried out at carefully selected airports across Indonesia's major islands, comprising diverse geographical and climatic conditions, including Sumatra, Java, Kalimantan, Bali, Nusa Tenggara, Maluku Islands, Sulawesi, and Papua, as shown in Figure 2. Elevation was a key consideration in site selection due to its influence on ambient temperature and effect on pavement temperature distribution. Each airport featured distinct pavement characteristics, with asphalt layer thickness varying based on the types of aircraft served. Airports handling narrow-body aircraft such as Boeing 737 and Airbus A320 typically had asphalt layers of 15 cm thick, while those serving wide-body aircraft, including Boeing 777 and Airbus A330, required thicker layers of 16-20 cm. These thickness differences affected temperature distribution in pavement layers, serving as an essential focus of the study. Temperature sensors were installed at multiple depths, from the surface to the binder layers, to provide a comprehensive mapping of pavement temperature distribution. The location of selected airports and their elevations are presented in Figure 3. The selected airports are across major islands in Indonesia, including Sumatra, Java, Kalimantan, Bali, Nusa Tenggara, Maluku Islands, Sulawesi, and Papua. This selection ensured geographical diversity, covering regions with varying elevations and climatic conditions, such as coastal lowlands and high-altitude mountainous areas.

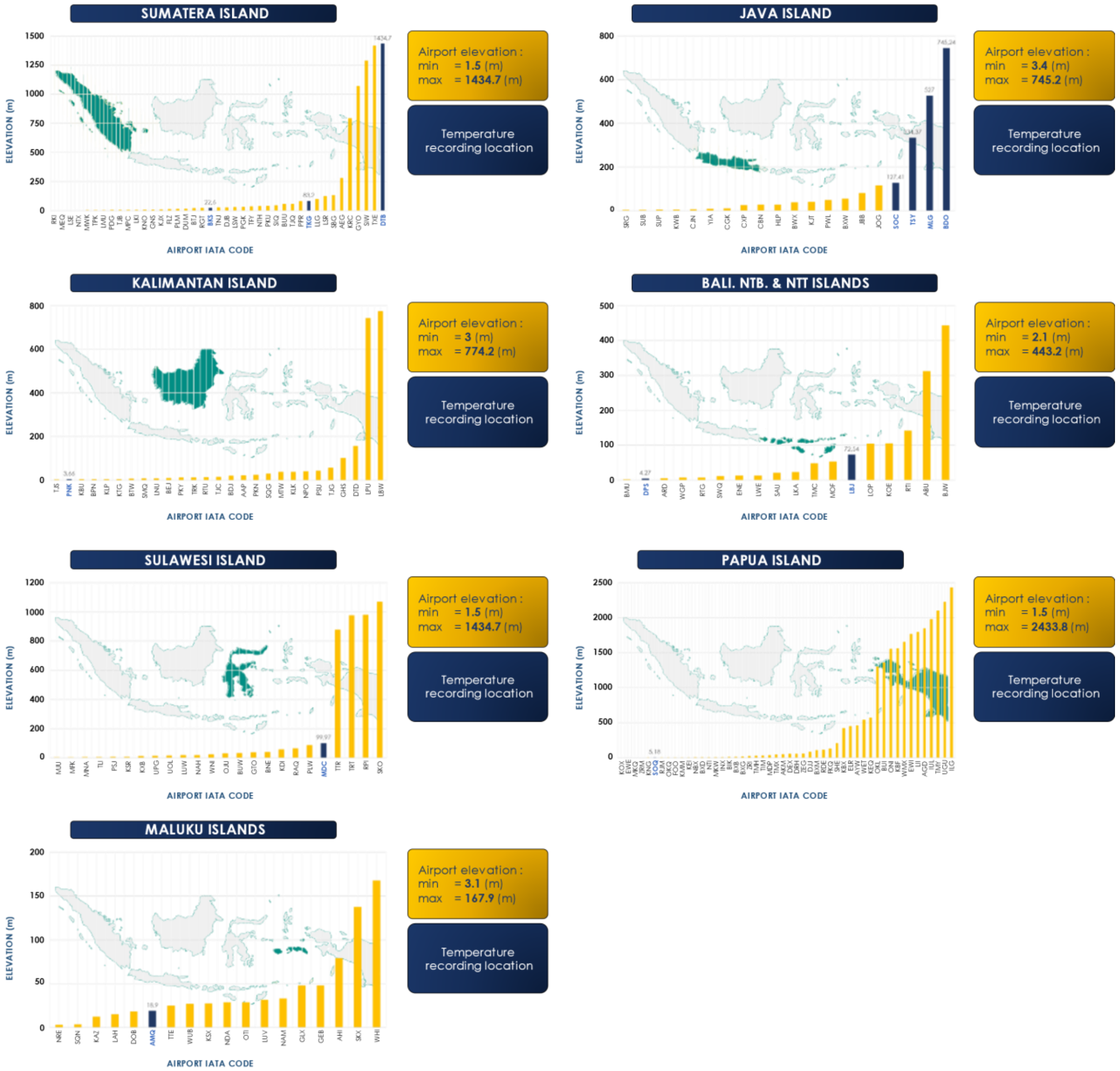


**Figure 2. Airport elevation distribution in Indonesia**

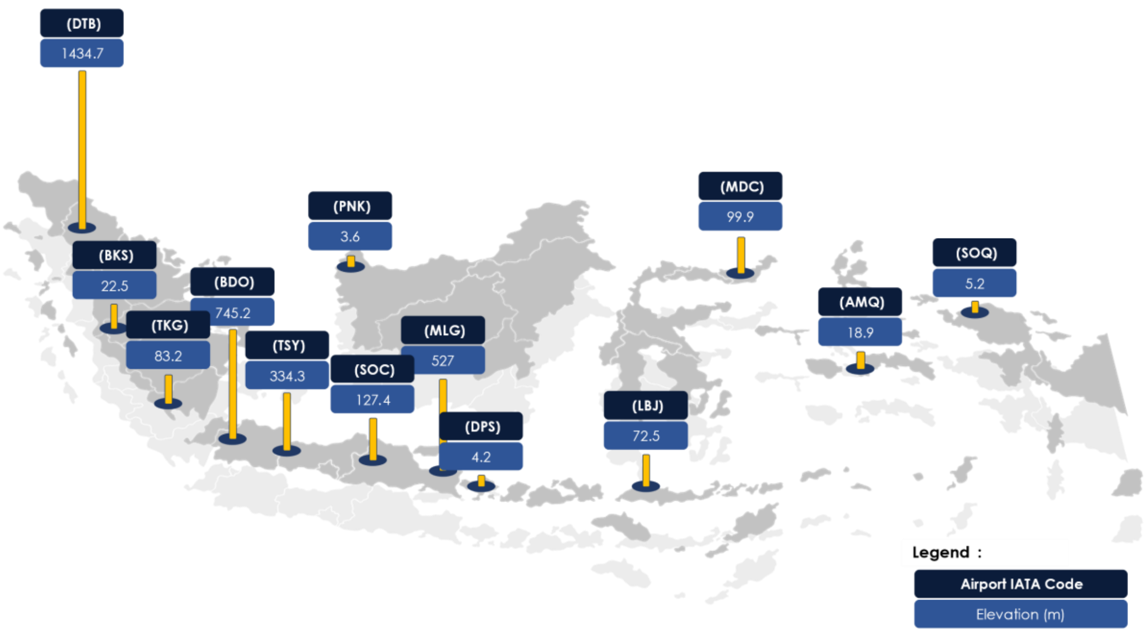


**Figure 3. Map of selected airports for pavement temperature observations**

# 6. Airside Pavement Sensing System (AirPaSS)

## 6.1. AirPaSS Design

Pavement temperature profile was measured using AirPaSS, a device specifically designed for monitoring in airport airside areas. Compared to previous studies [28, 29], which depended on limited datasets, this study used real-time data streams to enhance the accuracy and reliability of temperature monitoring. This method allowed for continuous updates to the predictive model, capturing temporal variations in environmental and operational conditions that could be overlooked by previous models. Moreover, the integration of AirPaSS enables more precise calibration and validation of predictive models, accounting for extreme temperature variations and high thermal loads characteristic of tropical climates. By combining real-time data integration with predictive modeling, it connects the gap between theoretical studies and operational needs, providing a scalable solution for enhancing pavement performance and lifespan in tropical regions. The physical design features comprising a panel box equipped with a solar panel on top are shown in Figure 4. Figure 5 shows the example of the AirPaSS installation at one of the airports. The design ensures optimal functionality for monitoring pavement temperatures at airports. The device integrates various components to accurately collect, process, and report temperature data. Since AirPaSS is used in active airside areas, it adheres to several critical criteria:

- **Frangible Design** - The device is designed to break into fragments upon impact by vehicles or aircraft, minimizing risks to flight operations.
- **Self-Powered** - The device operates independently, utilizing its own power source, as it is installed in airside areas without access to external electrical cables.
- **Real-Time Data Transmission -** Due to the continuous nature of airport operations, the device eliminates the need for manual data retrieval by autonomously transmitting data to a server system in real-time.

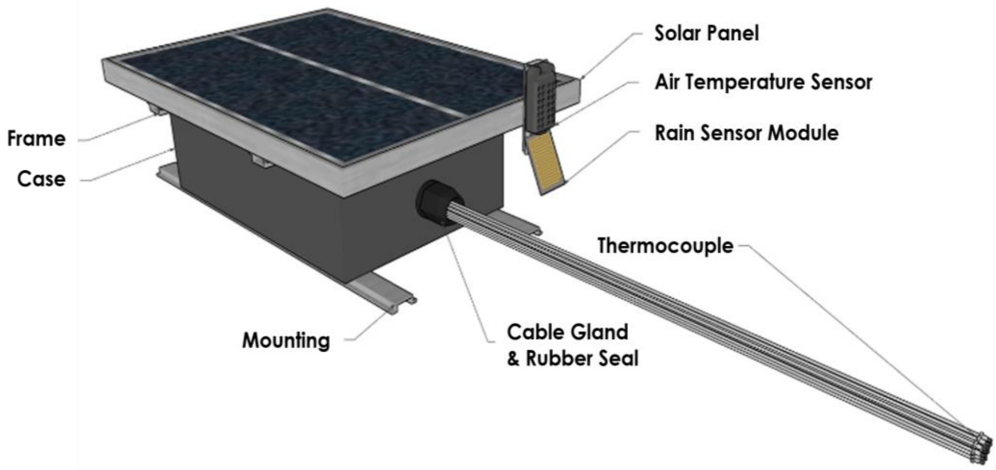


**Figure 4. AirPaSS isometric design**

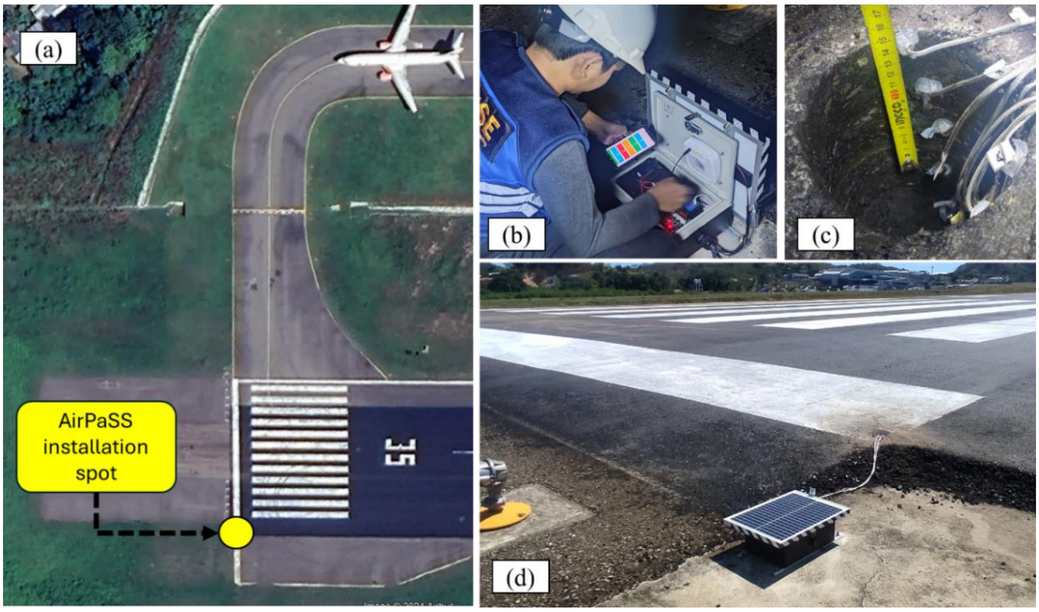


**Figure 5. (a) AirPaSS installation spot at Komodo International Airport (LBJ), (b) device setting, (c) sensor placement, (d) installed device**

The AirPaSS device comprises various integrated components designed to meet operational criteria in active airside areas. It features thermocouple sensors embedded at different pavement depths to measure temperatures in a range of 0-400°C, connected to a mainboard for data processing and Wi-Fi-based communication. A GSM modem with LTE capability ensures real-time data transmission, while a solar panel powers the system, supported by a rechargeable Valve-Regulated Lead Acid (VRLA) battery. Additional features include a rain detection module, which classifies weather conditions, and an air temperature sensor (DHT21) for ambient monitoring. The device is designed for durability, self-sufficiency, and reliable performance in remote, high-demand airport environments.

## 6.2. AirPaSS Workflow

The AirPaSS system is designed to provide accurate real-time pavement temperature data through an automated workflow, as shown in Figure 6. Thermocouple sensors embedded at various pavement depths detect temperature, which is converted from analog to digital signals by the IC MAX6675 and processed through a microcontroller. Temperature readings are stored in temporary memory every second, which are processed and transmitted through a microcontroller to a server using an integrated communication system. The server stores the data in a structured database every 15 minutes to allow accessibility for analysis and visualization through a web-based dashboard. Users can monitor temperature trends, changes, or critical conditions effortlessly. This workflow operates on a scheduled loop, ensuring data is consistently updated. Additionally, the system uses smart energy management, powered by solar panels and rechargeable batteries, ensuring uninterrupted operation.

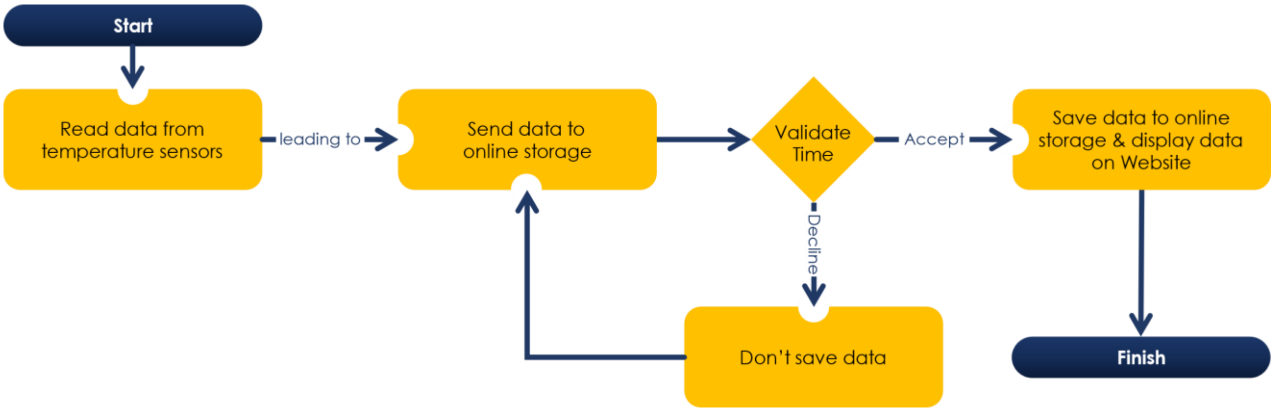


**Figure 6. AirPaSS workflow**

## 6.3. Data Storage and Presentation

AirPaSS uses a MySQL database to store data, structured into tables with columns such as ID, date, temperature, weather, and battery status. On the server side, PHP facilitates interactions with the MySQL database, enabling data storage and retrieval. The microcontroller transmits temperature data to the server through a predefined communication protocol, which PHP processes and stores in the database, including details such as date, temperature, weather conditions, and battery level ("2023-11-23 08:30:00, 28.5°C, Sunny, 80%"). The web dashboard, developed using PHP, provides a dynamic and responsive interface. Furthermore, it retrieves data from the MySQL database to show structured information and graphical temperature trends over time. Features include selecting specific date ranges for viewing temperature and weather data, a search function for finding specific records, and user authentication to restrict access to authorized users. PHP also processes battery level data to visually represent its status on the dashboard. Responsive design ensures compatibility across devices, including desktops and mobile devices, offering an intuitive user interface. Through the integration of PHP and MySQL, the AirPaSS dashboard delivers a secure, user-friendly platform for data analysis, enabling better decision-making based on accurate temperature, weather, and battery condition data.

## 6.4. Calibration for AirPaSS Quality Control

Thermocouple calibration in the AirPaSS microcontroller is conducted by comparing the readings with those of a mercury thermometer, considered a standard due to high accuracy. Both devices are placed in the same environment to ensure identical exposure to temperature. Subsequently, temperature readings from the thermocouple and the mercury thermometer are recorded simultaneously. These differences (deviations) are analyzed to understand the thermocouple's response and deviation patterns.

Based on the analysis, a mathematical equation representing the correction required for accurate thermocouple readings is derived (Figure 7). The calibration equation is integrated into the microcontroller program to adjust thermocouple readings automatically. The process passes through validation, comparing the corrected thermocouple readings against the mercury thermometer's measurements to ensure accuracy. This causes improvement in the reliability of temperature data collected by AirPaSS, providing a solid foundation for monitoring pavement temperatures at airports.

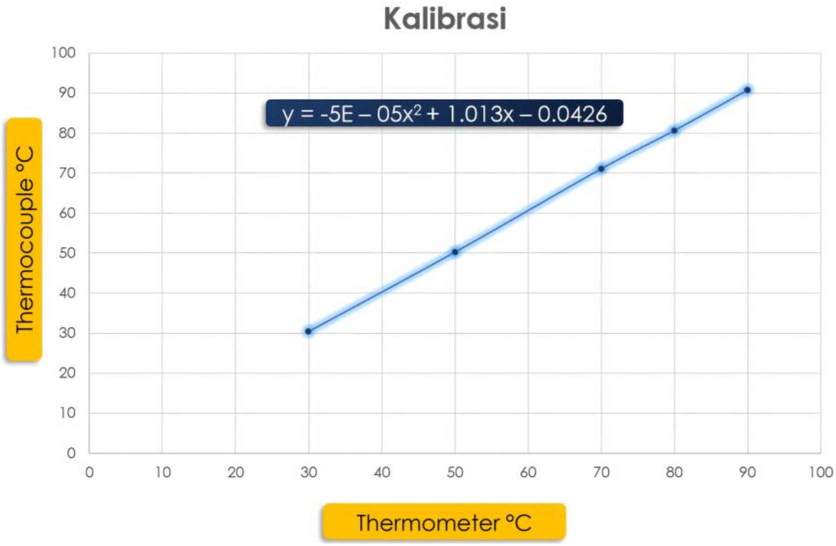


**Figure 7. Calibration graph of thermocouple-thermometer reading**

## 6.5. Temperature Data Processing

Temperature data collected by the sensors is processed by an onboard microcontroller and transmitted to a server using a portable Wi-Fi connection integrated in the data logging device. The system ensures continuous data processing, with temperature readings automatically sent to the server. Users can conveniently access and analyze the stored data through a dynamic, web-based dashboard, enabling real-time monitoring and visualization of temperature trends (see Figures 8 and 9).

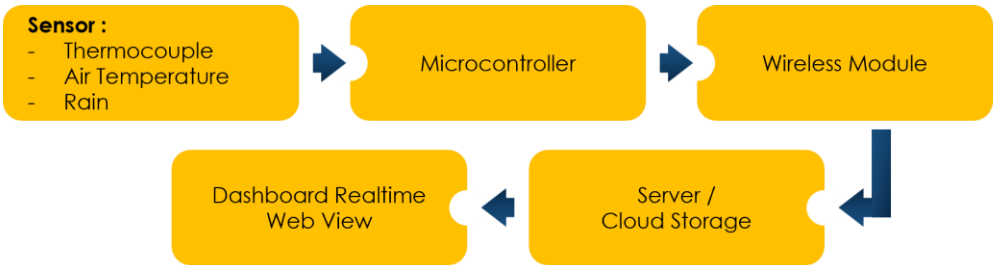


**Figure 8. Data processing flow**

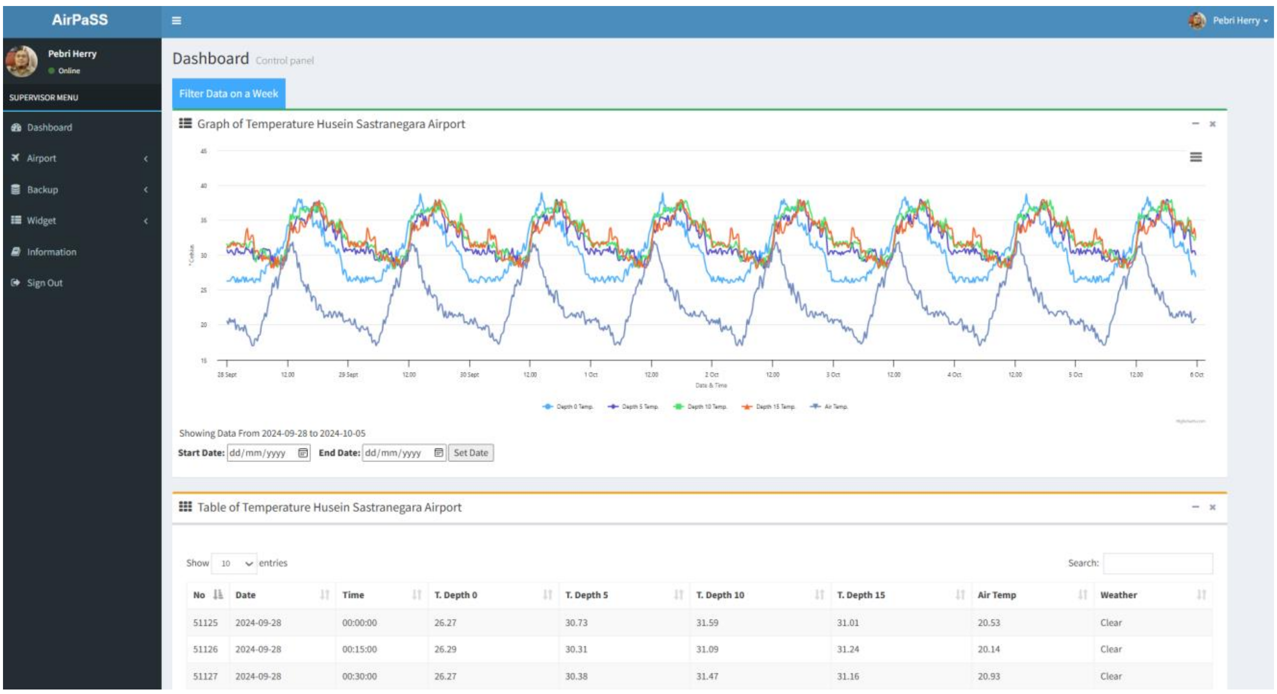


**Figure 9. Example of web-based temperature data display**

The dashboard provides a comprehensive interface, visualizing temperature trends while showing the data logger's battery status to ensure uninterrupted device operation during data collection. All data is securely stored in a database, accessible only to authorized users, with regular backups implemented to safeguard against data loss. Users can export data in CSV format for advanced analysis and integration with other tools. To uphold data integrity, raw data are subjected to rigorous analysis for potential technical errors, such as sensor malfunctions or recording inaccuracies. Outliers, which are data points significantly deviating from expected trends, are flagged for further investigation. When the data is determined to be an error caused by technical issues, outliers are either excluded or corrected to preserve the accuracy of the analysis. By combining real-time data processing, secure storage, and proactive error management, the AirPaSS system delivers reliable and high-quality temperature monitoring essential for pavement analysis and decision-making.

### 6.6. AirPaSS Long Term Reliability

Long-term reliability of AirPaSS is significantly enhanced through the integration of ESP32 microcontrollers and VRLA batteries. The combination of the two technologies offers a reliable, energy-efficient solution for Internet of Things (IoT) systems, enhancing performance and ensuring operational continuity in diverse environments. ESP32 is known for flexibility, energy efficiency, and wireless connectivity, serving as a suitable option for applications in environmental monitoring and automation [31, 32]. The power management features, such as sleep modes, further reduce energy consumption. In sensor-based systems, including AirPaSS, ESP32 efficiently manages data collection and transmission, ensuring long-term operation. Christopher et al. [33] showed the versatility of integrating ESP32 with sensors such as DHT11 for real-time control in smart systems.

VRLA batteries serve as dependable backup power for IoT devices, although there is potential degradation due to lead sulfate crystal build-up [34]. This issue can be reduced by Pulse Width Modulation (PWM) charging technology, thereby extending battery life, with predictive methods detecting potential failures early [35]. Combining solar panels with VRLA batteries in systems such as AirPaSS ensures autonomous operation, optimizing energy flow through ESP32. This integration improves system reliability and efficiency in remote or harsh environments. Additionally, proper temperature and voltage control [36] further extends battery life, ensuring consistent performance in challenging conditions. In terms of sensors, AirPaSS sensors use Type K thermocouples, known for their long-term reliability and accuracy. Type K thermocouples are widely used for temperature measurements of approximately 1260°C (2300°F), showing suitability for extreme conditions. Compared to other types of thermocouples, Type K offers a longer lifespan due to its better resistance against rapid oxidation at higher temperatures.

## 7. Selection of Parameters Influencing Maximum Temperatures

Pavement temperature distribution is influenced by a complex interplay of environmental factors, including air temperature, solar radiation, atmospheric heat transfer, long-wave radiation, cloud cover, relative humidity, wind speed, and rainfall intensity [13]. Among these factors, cloud cover, humidity, wind, and rainfall have indirect effects on pavement temperature by modulating air temperature and solar radiation, which are the primary determinants of thermal behavior in pavement systems (Figure 10).

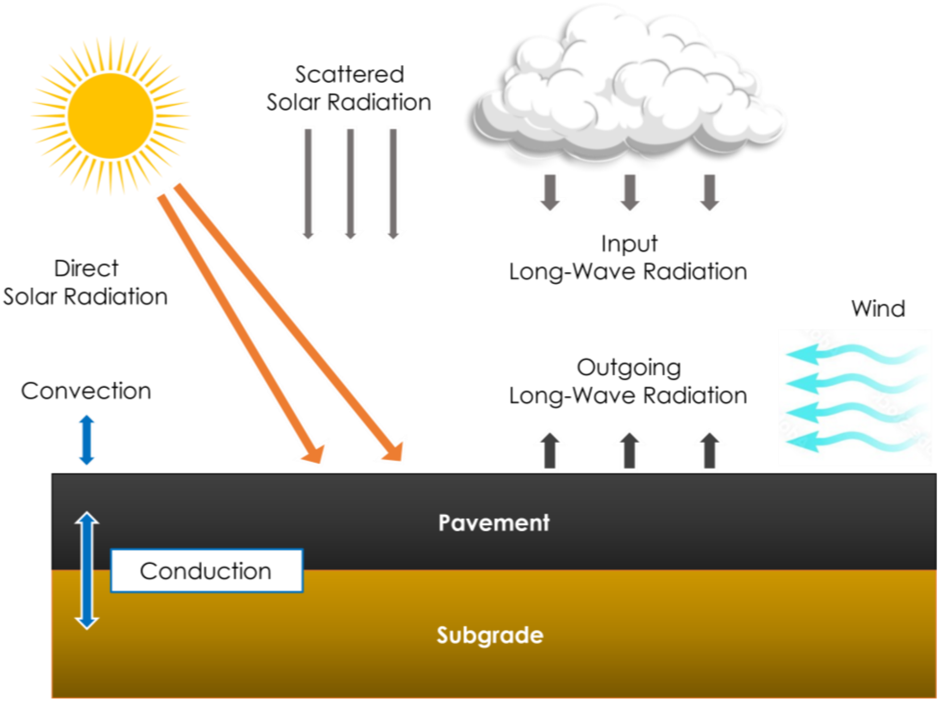


**Figure 10. Environmental factors to pavement temperatures [12]**

Atmospheric heat transfer and long-wave radiation are challenging to monitor directly due to their significant dependence on air temperature, which serves as a reliable proxy for environmental factors [12]. Additionally, studies have shown the significant influence of elevation on solar radiation and air temperature [37]. At higher elevations, solar radiation increases proportionally due to the thinner atmospheric layer that reduces scattering and absorption. Despite the higher solar radiation, air temperature decreases with elevation because of the adiabatic cooling effect, where the air cools as it expands in lower-pressure environments. This inverse relationship suggests that elevation can effectively substitute solar radiation as a factor in modeling pavement temperature. Therefore, by incorporating air temperature and elevation as independent environmental variables inside the developed predictive model, there is a possibility to capture the key drivers of pavement temperature distribution while simplifying data requirements. These substitutions enhance the practical application of models and improve the accuracy of temperature distribution predictions in pavement systems.

## 8. Effect of Air Temperature on Pavement Temperature Distribution

Air temperature is the most dominant environmental variable influencing the temperature distribution in asphalt pavement layers. Lukanen et al. [5] and Huang [38] showed that air temperature significantly affects the stiffness of asphalt mixtures, influencing the structural performance of pavements. This study examines how daily air temperature variations influence temperatures at various pavement depths across 13 airports. RDO Asphalt 09/24 [39] provides an important theoretical foundation for understanding how air temperature affects the temperature distribution within pavements. Based on the logarithmic regression model developed, the temperature decrease at pavement depth follows a distinct pattern, represented by the following equation:

$$T_{pav,d} = b\ln(0.01d + 1) + T_{surf} \tag{1}$$

where $b$ is empirical coefficient factor related to surface temperature, $d$ is pavement depth, in mm, and $T_{surf}$ is surface temperature of the pavement, in °C (Table 1).

**Table 1. Value of coefficient *b***

| Surface Temperature, °C | <-10 | <-5 | < 0 | < 5 | < 10 | < 15 | < 20 | < 25 | < 30 | < 35 | < 40 | < 45 | >45 |
|---|---|---|---|---|---|---|---|---|---|---|---|---|---|
| Value of b | 6.5 | 4.5 | 2.5 | 0.7 | 0.1 | 0.3 | 0.4 | -1.6 | -4.0 | -6.2 | -8.5 | -10.5 | -12.0 |

The formula describes a logarithmic decline in temperature with increasing pavement depth, which stabilizes at greater depth. This phenomenon is attributed to slower thermal conduction in the lower pavement layers, which are more insulated from surface air temperature fluctuations. Observations from the 13 airports support this model, showing significant maximum temperature reductions in the surface and shallow layers of pavement (0-5 cm). This temperature decrease gradually slows and stabilizes at greater depths. The correlation of asphalt pavement temperature and their depth is shown in Figure 11. This indicates that the relationship between maximum pavement temperatures and depth follows a natural logarithmic trend.

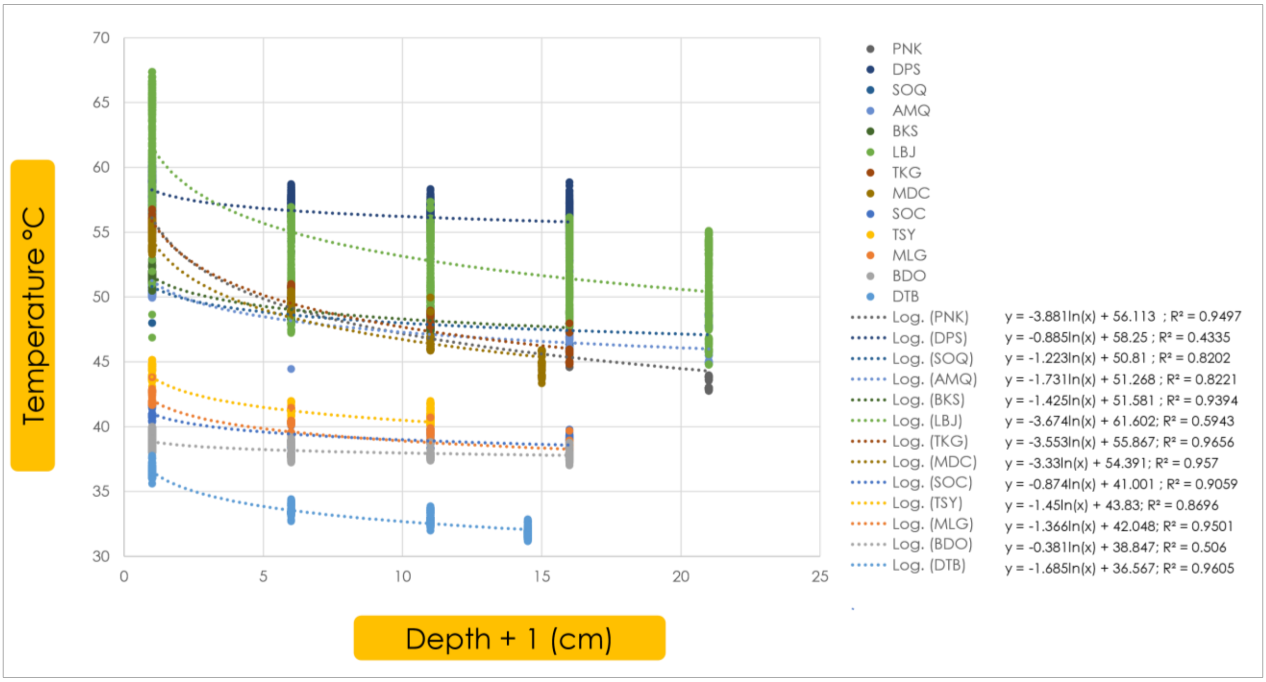


**Figure 11. Correlation of maximum asphalt pavement temperature and depth at Indonesian airports**

## 9. Effect of Airport Elevation on Pavement Temperature Distribution

Airport elevation is a key variable influencing temperature distribution in flexible pavements, particularly in surface layers. Based on the analysis shown in Figure 12, the relationship between elevation and the surface temperature of asphalt pavements follows a significant logarithmic correlation pattern. This correlation shows a decreasing temperature trend with increasing airport elevation, both for maximum and average temperature.

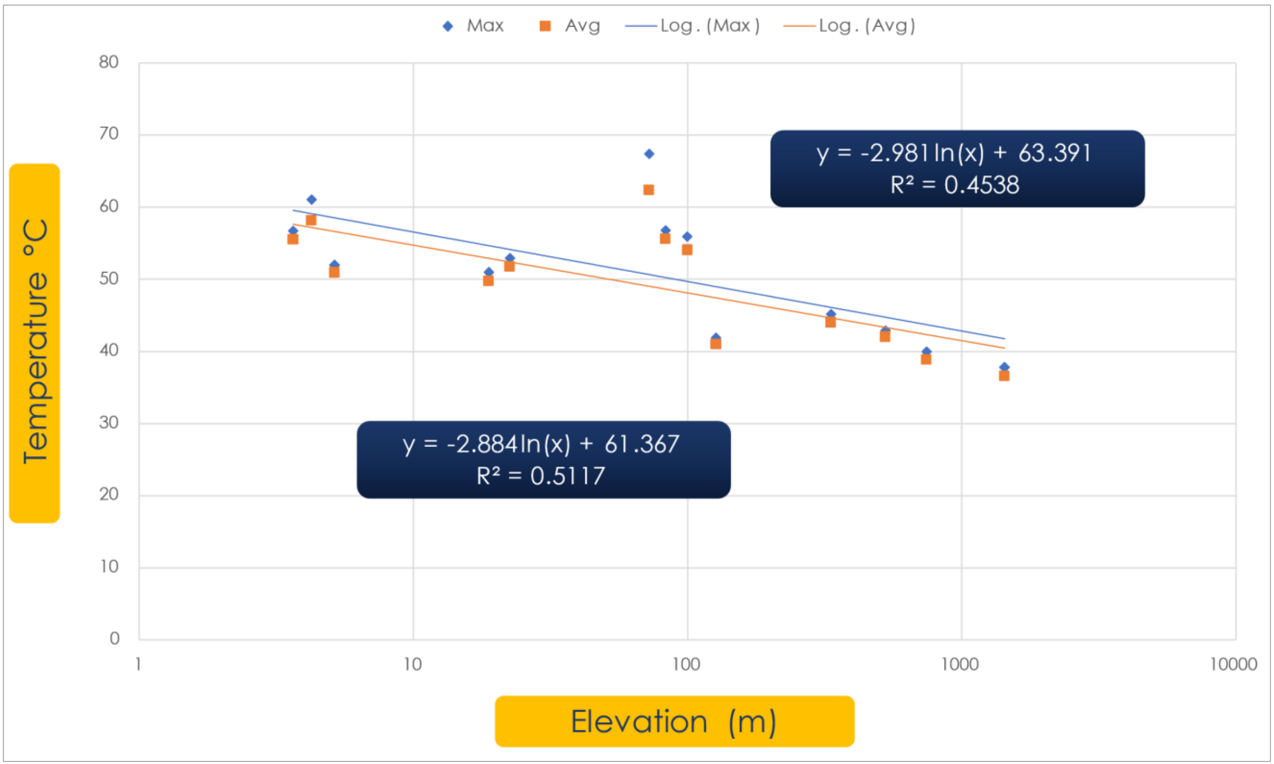


**Figure 12. Correlation between asphalt pavement surface temperature and airport elevation**

The logarithmic regression curve for maximum temperatures shows that elevation has a more significant impact on the reduction of maximum pavement temperature, with a coefficient of determination ($R^2$) value of 0.5117. Meanwhile, the regression curve for average temperatures obtains $R^2$ value of 0.4538.

Based on the correlation, airports located in low-elevation areas tend to show higher and more fluctuating pavement surface temperatures. However, airports at higher elevations show a more stable temperature distribution pattern, with lower values.

## 10. Clustering of Pavement Temperature for Indonesia

The development of airports clustering based on temperature distribution is an essential step in this study to understand the climatic and environmental characteristics influencing the performance of flexible pavements. This clustering is designed to classify airports in Indonesia according to similarities in temperature distribution patterns, enabling pavement material planning to be better tailored to the specific environmental conditions of each location. Previous studies also attempted to create clustering of pavement temperatures for design purposes as presented by Zeiada et al. [23] and Kleizienė et al. [40].

To classify airports based on similarities in temperature distribution characteristics, the complete linkage method was used in hierarchical cluster analysis. This method was selected to allow grouping of airports based on the distance or similarity between data sets, measured using a defined set of determining parameters [40]. Subsequently, the maximum distance between datasets for each airport was calculated, enabling more accurate clustering to identify airports with similar temperature distribution patterns. In this study, the key parameters used for developing clusters include (see Table 2):

- Average maximum air temperature ($T_1$),
- Average maximum surface pavement temperature ($T_2$), and
- Average maximum pavement temperature at a depth of 5 cm ($T_3$).

These three parameters were selected due to their direct influence on the temperature distribution in asphalt pavements, providing a comprehensive depiction of the interaction between the environment and pavement. In determining the similarity of clustering parameters, the Euclidean distance between airports X and Y, with a total of n determining parameters, is defined as the sum of the squared differences between the parameters. The formula is illustrated as follows:

$$Euclidean\ Dist._{(X,Y)} = \sqrt[2]{\sum_{i=1}^{n}(T_{iX} - T_{iY})^2} \tag{2}$$

The matrix of Euclidean distances among airports is shown in Table 3.

**Table 2. Temperature data for airports in hierarchical cluster analysis using complete linkage**

| ID | Airport Name | IATA Code | Elevation (m) | Average Maximum Air Temperature (°C) / ($T_1$) | Average Maximum Surface Pavement Temperature (°C) / ($T_2$) | Average Maximum 5-cm-depth Pavement Temperature (°C) / ($T_3$) |
|---|---|---|---|---|---|---|
| 1 | Komodo | LBJ | 72.54 | 35.84 | 62.37 | 53.08 |
| 2 | I Gusti Ngurah Rai | DPS | 4.27 | 33.97 | 58.14 | 56.97 |
| 3 | Radin Inten II | TKG | 83.21 | 33.46 | 55.59 | 50.01 |
| 4 | Sam Ratulangi | MDC | 99.97 | 33.55 | 54.07 | 49.48 |
| 5 | Supadio | PNK | 3.66 | 33.47 | 55.52 | 50.02 |
| 6 | Domino Eduard Osok | SOQ | 5.18 | 30.35 | 50.90 | 48.50 |
| 7 | Silangit | DTB | 1435.69 | 28.46 | 36.56 | 33.46 |
| 8 | Pattimura | AMQ | 18.90 | 32.36 | 49.73 | 49.49 |
| 9 | Fatmawati Soekarno | BKS | 22.56 | 31.36 | 51.7 | 48.79 |
| 10 | Adi Soemarmo | SOC | 127.41 | 32.38 | 40.98 | 39.47 |
| 11 | Wiriadinata | TSY | 334.37 | 28.62 | 43.99 | 40.61 |
| 12 | Abdurrahman Soleh | MLG | 527.00 | 31.54 | 42.01 | 39.59 |
| 13 | Husein Sastranegara | BDO | 745.24 | 30.92 | 38.85 | 38.19 |

**Table 3. Initial Euclidean distance matrix of the airports based on key parameters**

| ID | 1 | 2 | 3 | 4 | 5 | 6 | 7 | 8 | 9 | 10 | 11 | 12 | 13 |
|---|---|---|---|---|---|---|---|---|---|---|---|---|---|
| 1 | 0.00 | 6.04 | 7.81 | 9.33 | 7.87 | 13.52 | 33.25 | 13.59 | 12.34 | 25.59 | 23.35 | 24.80 | 28.27 |
| 2 | 6.04 | 0.00 | 7.43 | 8.53 | 7.44 | 11.72 | 32.38 | 11.37 | 10.73 | 24.56 | 22.28 | 23.84 | 27.09 |
| 3 | 7.81 | 7.43 | 0.00 | 1.61 | 0.07 | 5.83 | 25.71 | 5.98 | 4.59 | 18.05 | 15.70 | 17.22 | 20.65 |
| 4 | 9.33 | 8.53 | 1.61 | 0.00 | 1.55 | 4.61 | 24.27 | 4.50 | 3.30 | 16.52 | 14.30 | 15.73 | 19.13 |
| 5 | 7.87 | 7.44 | 0.07 | 1.55 | 0.00 | 5.78 | 25.67 | 5.92 | 4.53 | 18.00 | 15.65 | 17.18 | 20.60 |
| 6 | 13.52 | 11.72 | 5.83 | 4.61 | 5.78 | 0.00 | 20.87 | 2.53 | 1.32 | 13.57 | 10.63 | 12.64 | 15.87 |
| 7 | 33.25 | 32.38 | 25.71 | 24.27 | 25.67 | 20.87 | 0.00 | 21.11 | 21.74 | 8.43 | 10.31 | 8.76 | 5.80 |
| 8 | 13.59 | 11.37 | 5.98 | 4.50 | 5.92 | 2.53 | 21.11 | 0.00 | 2.32 | 13.30 | 11.22 | 12.58 | 15.75 |
| 9 | 12.34 | 10.73 | 4.59 | 3.30 | 4.53 | 1.32 | 21.74 | 2.32 | 0.00 | 14.24 | 11.57 | 13.36 | 16.66 |
| 10 | 25.59 | 24.56 | 18.05 | 16.52 | 18.00 | 13.57 | 8.43 | 13.30 | 14.24 | 0.00 | 4.95 | 1.33 | 2.88 |
| 11 | 23.35 | 22.28 | 15.70 | 14.30 | 15.65 | 10.63 | 10.31 | 11.22 | 11.57 | 4.95 | 0.00 | 3.67 | 6.13 |
| 12 | 24.80 | 23.84 | 17.22 | 15.73 | 17.18 | 12.64 | 8.76 | 12.58 | 13.36 | 1.33 | 3.67 | 0.00 | 3.51 |
| 13 | 28.27 | 27.09 | 20.65 | 19.13 | 20.60 | 15.87 | 5.80 | 15.75 | 16.66 | 2.88 | 6.13 | 3.51 | 0.00 |

An example of the calculation is provided below to show the methodology. Consider the comparison between Komodo International Airport (LBJ, ID: 1) and I Gusti Ngurah Rai International Airport in Denpasar (DPS, ID: 2). This pairing serves as an example to show the step-by-step process of evaluating the relationship between the two data points in the dataset.

$$Euclidean\ Dist._{(1,2)} = \sqrt[2]{(35.84 - 33.97)^2 + (62.37 - 58.14)^2 + (53.08 - 56.97)^2} \tag{3}$$

$$Euclidean\ Dist._{(1,2)} = 6.04 \tag{4}$$

The calculation process starts by identifying the minimum value in the dataset, followed by combining the corresponding row and column IDs. Subsequently, these IDs are merged into a single cluster, retaining the maximum value among the elements. The new Euclidean distance matrix is created, which is shown in Table 4. The procedure iteratively locates the next minimum value and continues until all elements are grouped into clusters. A detailed summary of the complete linkage solution is shown in Table 5.

**Table 4. Euclidean distance matrix of the airports based on key parameters – phase 2**

| ID | 1 | 2 | {3,5} | 4 | 6 | 7 | 8 | 9 | 10 | 11 | 12 | 13 |
|---|---|---|---|---|---|---|---|---|---|---|---|---|
| 1 | 0.00 | 6.04 | 7.87 | 9.33 | 13.52 | 33.25 | 13.59 | 12.34 | 25.59 | 23.35 | 24.80 | 28.27 |
| 2 | 6.04 | 0.00 | 7.44 | 8.53 | 11.72 | 32.38 | 11.37 | 10.73 | 24.56 | 22.28 | 23.84 | 27.09 |
| {3,5} | 7.87 | 7.44 | 0.00 | 1.61 | 5.83 | 25.71 | 5.98 | 4.59 | 18.05 | 15.70 | 17.22 | 20.65 |
| 4 | 9.33 | 8.53 | 1.61 | 0.00 | 4.61 | 24.27 | 4.50 | 3.30 | 16.52 | 14.30 | 15.73 | 19.13 |
| 6 | 13.52 | 11.72 | 5.83 | 4.61 | 0.00 | 20.87 | 2.53 | 1.32 | 13.57 | 10.63 | 12.64 | 15.87 |
| 7 | 33.25 | 32.38 | 25.71 | 24.27 | 20.87 | 0.00 | 21.11 | 21.74 | 8.43 | 10.31 | 8.76 | 5.80 |
| 8 | 13.59 | 11.37 | 5.98 | 4.50 | 2.53 | 21.11 | 0.00 | 2.32 | 13.30 | 11.22 | 12.58 | 15.75 |
| 9 | 12.34 | 10.73 | 4.59 | 3.30 | 1.32 | 21.74 | 2.32 | 0.00 | 14.24 | 11.57 | 13.36 | 16.66 |
| 10 | 25.59 | 24.56 | 18.05 | 16.52 | 13.57 | 8.43 | 13.30 | 14.24 | 0.00 | 4.95 | 1.33 | 2.88 |
| 11 | 23.35 | 22.28 | 15.70 | 14.30 | 10.63 | 10.31 | 11.22 | 11.57 | 4.95 | 0.00 | 3.67 | 6.13 |
| 12 | 24.80 | 23.84 | 17.22 | 15.73 | 12.64 | 8.76 | 12.58 | 13.36 | 1.33 | 3.67 | 0.00 | 3.51 |
| 13 | 28.27 | 27.09 | 20.65 | 19.13 | 15.87 | 5.80 | 15.75 | 16.66 | 2.88 | 6.13 | 3.51 | 0.00 |

**Table 5. Summary of hierarchical cluster analysis using complete linkage**

| Fase | ID Group 1 | ID Group 2 | Euclidean Distance |
|---|---|---|---|
| 1 | 3 | 5 | 0.0714 |
| 2 | 6 | 9 | 1.3207 |
| 3 | 10 | 12 | 1.3345 |
| 4 | {3,5} | 4 | 1.6123 |
| 5 | {6,9} | 8 | 2.5277 |
| 6 | {10,12} | 13 | 3.5114 |
| 7 | {{3,5},4} | {{6,9},8} | 5.9850 |
| 8 | 1 | 2 | 6.0433 |
| 9 | {{10,12},13} | 11 | 6.1291 |
| 10 | 7 | {{{10,12},13},11} | 10.3128 |
| 11 | {1,2} | {{{3,5},4},{{6,9},8}} | 13.5929 |
| 12 | {{1,2},{{{3,5},4},{{6,9},8}}} | {{{{10,12},13},11},7} | 33.2500 |

The final output is a dendrogram, a hierarchical diagram showing the relationships between airports with similar temperature distribution patterns. The dendrogram, shown in Figure 13, provides a clear visual representation of airport groupings based on the parameters used to define airport cluster.

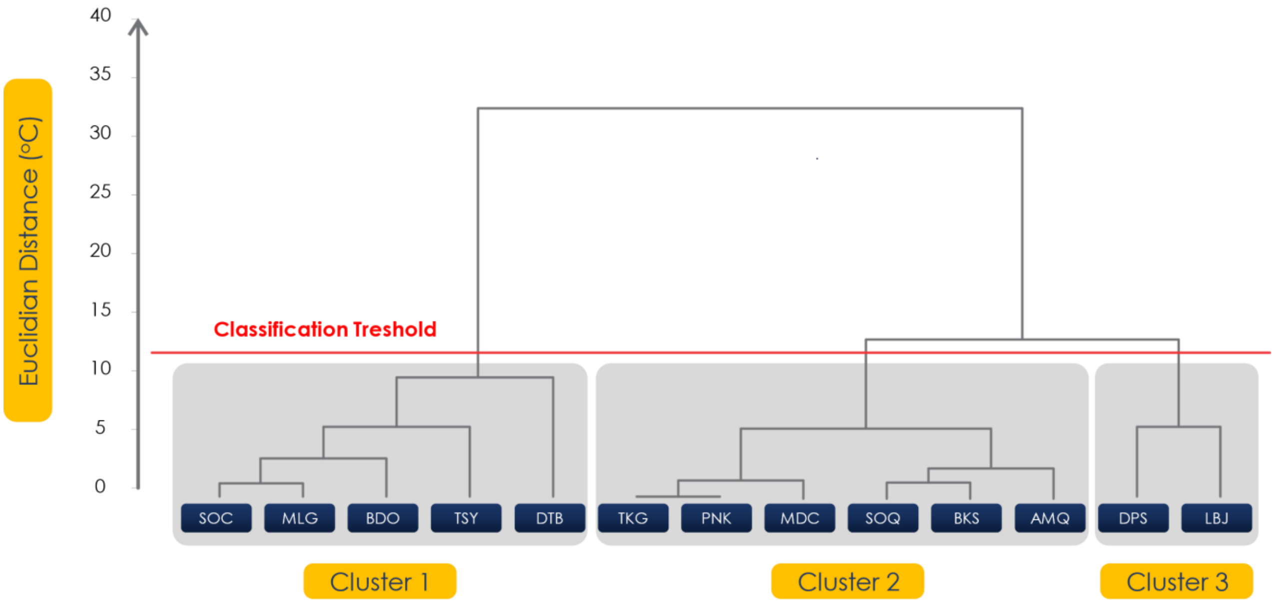


**Figure 13. Dendrogram of airport classification using the complete linkage method**

Based on the dendrogram, airport classification can be divided into three clusters, with each group sharing similar environmental characteristics and asphalt pavement temperature distribution patterns. Therefore, airports in this study are grouped into several clusters of climate and temperature distribution. Each cluster possesses unique characteristics in terms of air temperature range and distribution in pavement layers, which serve as the basis for selecting more appropriate pavement materials.

The general characteristics of the clusters are further analyzed as shown in Table 6, with their classification presented in Table 7. As shown in Figure 14, all airports in Clusters 2 and 3 are located below 100 meters in elevation, showing significant features from the higher-elevation airports in Cluster 1. Based on Figure 15, the average maximum air temperature and surface temperature differentiate Cluster 2 from Cluster 3, with the threshold set at 33.8°C and 57°C, respectively. These temperature thresholds show the distinct environmental conditions of airport pavements in each cluster.

**Table 6. General characteristics of airport's clusters**

| Airport Name | IATA Code | Elevation (m) | Average Maximum Air Temperature in 1 Year Period (°C) | Average Maximum Surface Temperature in 1-Year Period (°C) |
|---|---|---|---|---|
| | | **Cluster 1** | | |
| Adi Soemarmo | SOC | 127.41 | 32.38 | 40.98 |
| Abdurrahman Soleh | MLG | 527.00 | 31.54 | 42.01 |
| Husein Sastranegara | BDO | 745.24 | 30.92 | 38.85 |
| Wiriadinata | TSY | 334.37 | 28.62 | 43.99 |
| Silangit | DTB | 1435.69 | 28.46 | 36.56 |
| | | **Cluster 2** | | |
| Radin Inten II | TKG | 83.21 | 33.46 | 55.59 |
| Supadio | PNK | 3.66 | 33.47 | 55.52 |
| Sam Ratulangi | MDC | 99.97 | 33.55 | 54.07 |
| Domino Eduard Osok | SOQ | 5.18 | 30.35 | 50.90 |
| Fatmawati Soekarno | BKS | 22.56 | 31.36 | 51.70 |
| Pattimura | AMQ | 18.90 | 32.36 | 49.73 |
| | | **Cluster 3** | | |
| I Gusti Ngurah Rai | DPS | 4.27 | 33.97 | 58.14 |
| Komodo | LBJ | 72.54 | 35.84 | 62.37 |

**Table 7. Classification of airports cluster**

| Aspects | Cluster 1 | Cluster 2 | Cluster 3 |
|---|---|---|---|
| Airport Elevation | E > 100 m | E < 100 m | |
| Average Maximum Air Temperature in 1 Year Period | All | T ≤ 33.8°C | T > 33.8°C |
| Average Maximum Surface Temperature in 1-Year Period | All | T ≤ 57°C | T > 57°C |


**Figure 14. Elevation threshold for airport clustering**

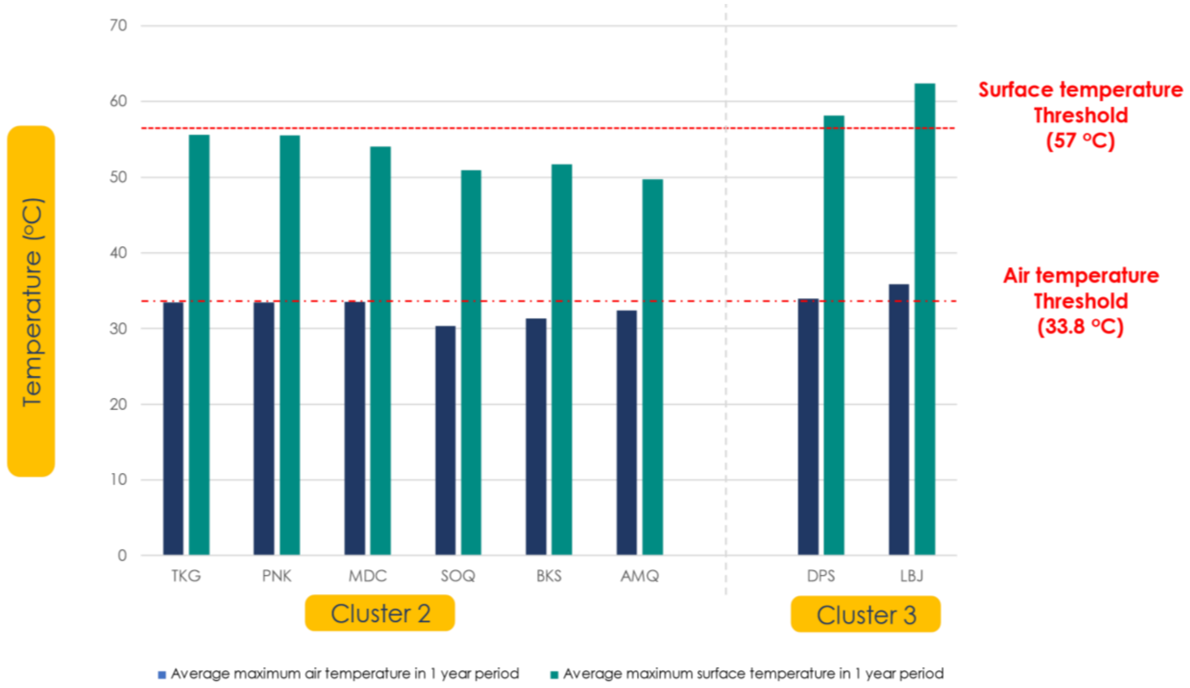


**Figure 15. Temperature threshold for airport clustering**

Based on the predefined airport clustering, the general characteristics of each cluster can be described as follows:

**1. Cluster 1**

Airports in Cluster 1 are located in highland or mountainous regions, with elevations exceeding 100 meters above sea level. The climatic conditions in these regions tend to be cooler, with stable and lower air temperatures compared to airports situated in lowland. Furthermore, the temperature distribution across the pavement surface layer is relatively moderate, reducing the risk of deformation caused by high temperatures.

**2. Cluster 2**

Airports are situated in lowland regions with moderate climatic conditions, characterized by relatively lower air and pavement surface temperatures compared to other clusters at similar elevations. This condition provides reduced thermal loads on pavement layers, allowing the use of standard asphalt mixture specifications while still achieving optimal performance.

**3. Cluster 3**

Airports in Cluster 3 are located in lowland regions but with hot tropical climates. Both air and pavement surface temperatures are significantly high, posing substantial challenges to the viscoelastic stability of asphalt mixtures. Consequently, airports in this cluster require pavement materials with high-temperature resistance specifications to mitigate the risk of permanent deformation, enhance durability under extreme temperatures, and ensure a longer pavement service life.

The characteristics of these clusters enable more precise pavement planning and design, focused on the climatic and elevation challenges faced by each airport.

## 11. Development of Pavement Temperature Distribution Model

A predictive model for maximum pavement temperature distribution was developed through a curve-fitting methodology using the dataset observations. The Nonlinear Generalized Reduced Gradient (Nonlinear GRG) algorithm was used to solve the optimization problem inherent in nonlinear models, ensuring the best solution in defined constraints. This method is well-suited for handling complex relationships between variables while maintaining adherence to physical and practical limitations [41]. The model formulation separates variables into dependent and independent categories, with constraints defined to express dependencies and simplify the problem structure. Independent variables are iteratively adjusted, while dependent variables are calculated according to the constraints. The optimization process evaluates the gradient of the target equation to determine the optimal direction for variable adjustments. Iterations continue until convergence is achieved, as shown by negligible changes in the optimized equation's value. Based on the insights derived from the dataset observations, the predictive model for pavement maximum temperature distribution is expressed as:

$$T_{pav,d}^{max} = \beta_D \ln(C_1 d + 1) + \beta_E \ln(C_2 E + 1) + C_3 T_{air} + C_4 \quad (5)$$

where $T_{air}$ is maximum air temperature, in °C, $d$ is pavement depth, in cm, and $E$ is airport elevation, in m, where the maximum-air-temperature-related coefficients, $\beta_D$ and $\beta_E$, are defined as:

$$\beta_D = a_1 T_{air} + a_2 \quad (6)$$

$$\beta_E = a_3 T_{air} + a_4 \quad (7)$$

The proposed formula represents a robust mathematical framework derived by analyzing observed trends in the dataset. It captures the interactions between key parameters such as pavement depth, airport elevation, and maximum air temperature in a coherent and structured manner. The inclusion of the maximum air temperature in the model shows the direct linear relationship between maximum air temperature and surface temperature at pavement level. This linearity is justified by the fact that surface temperature is strongly influenced by ambient air temperatures due to the thermal exchange processes of radiation, convection, and conduction.

At the surface level, the impact of air temperature is most pronounced because there are minimal material and environmental barriers between the air and pavement's exposed surface. This makes the maximum air temperature an effective proxy for predicting surface thermal conditions. Although the relationship between air temperature and surface temperature is linear, the effects of pavement depth and airport elevation are modeled logarithmically. Elevation impacts thermal gradients, but its effect diminishes at higher altitudes due to stabilizing atmospheric conditions.

By incorporating the relationships, the model balances linear and nonlinear components to provide a comprehensive representation of pavement thermal behavior. This enables accurate predictions critical for optimizing pavement design and maintenance strategies under varying environmental and climatic conditions. The proposed formula is purposefully designed to ensure practicality and usability compared to machine learning algorithms or other complex computational models, which often demand extensive datasets, significant computational power, and specialized expertise. By maintaining a simplified and robust structure, it serves as a highly accessible alternative, balancing computational efficiency with the precision required for practical applications in diverse scenarios.

The calibrated parameters $a_1$to $a_4$, and $C_1$ to $C_4$, denoted collectively as $\overline{X}$, are estimated through a curve-fitting approach. The parameters should minimize the error between the observed maximum pavement temperatures and predicted value. Therefore, the optimization problem based on *m* numbers of observed datasets could be stated as follows:

Objective Function:

$$\text{minimize } F(\overline{X}) = \sum_{j=1}^{m} \left( T_{pav,d}^{obs,j} - T_{pav,d}^{max,j}(\overline{X}) \right)^2 \quad (8)$$

Subject to the constraints:

$$a_1 \leq 0;\ a_3 \leq 0 \quad (9)$$

$$C_1 \geq 0;\ C_2 \geq 0\ ;\ C_3 \geq 0 \quad (10)$$

where $T_{pav,d}^{obs,j}$ is j$^{th}$ observed maximum temperature data at pavement depth *d*, in °C, and $T_{pav,d}^{max,j}(\overline{X})$ is j$^{th}$ predicted maximum temperature data at pavement depth *d* based on calibrated parameters $\overline{X}$ , in °C.

The method captures the relationship between maximum pavement temperature, air temperature, elevation, and depth while adhering to meaningful constraints. Iterative parameter refinement ensures robustness and predictive accuracy, offering a reliable framework for analyzing asphalt pavement temperature distributions. These constraints ensure that the maximum temperature distribution is in line with observed data, where maximum temperatures decrease with increasing pavement depth and airport elevation under various maximum air temperature scenarios. Additionally, $C_1$ and $C_2$ must be positive because the natural logarithmic function is undefined for negative values, which would disrupt the calibration process.

The model was developed based on data obtained from airports in each cluster, with the training and testing data for the pavement temperature predictive model comprising 70% and 30% of the available dataset, respectively. The use of a mixed linear and logarithmic regression model was based on trends observed in the dataset. The modeling method was selected because of the ability to provide sufficiently accurate results while maintaining ease of use, showing potential accessibility to practitioners outside of study fields. Based on the data, pavement temperatures in Indonesia had not dropped below 0°C. Therefore, the developed model focused only on predicting maximum pavement temperatures. Through a series of multivariable regression processes, the parameters for each cluster of the pavement temperature prediction model were developed and summarized in Table 8.

**Table 8. Parameters of the pavement maximum temperature distribution predictive model**

| Cluster Type | Optimized Parameters | | | | | | | |
|---|---|---|---|---|---|---|---|---|
| | $a_1$ | $a_2$ | $a_3$ | $a_4$ | $C_1$ | $C_2$ | $C_3$ | $C_4$ |
| Cluster 1 | -0.03746 | -0.36900 | 0.00000 | -34.57301 | 0.51671 | 0.00015 | 0.15000 | 38.83800 |
| Cluster 2 | -1.07235 | 30.24850 | -1.47683 | 0.00533 | 0.29127 | 0.00014 | 1.35726 | 9.78920 |
| Cluster 3 | -0.20633 | 5.45495 | -0.01000 | -2.55964 | 4.38711 | 0.01672 | 1.60466 | 5.73548 |

Figures 16 to 18 provide a detailed comparison between predicted pavement temperatures, derived from the proposed model, and the measured temperatures at various depths. The results validate the precision and reliability of Equation (3) and the parameters in Table 7 for predicting pavement temperatures across different depths. Specifically, the Cluster 1 model achieved a Root Mean Squared Error (RMSE) of 1.29°C and an Adjusted $R^2$ value of 0.80. The Cluster 2 model showed superior accuracy with an RMSE of 0.91°C and an adjusted $R^2$ value of 0.91. Cluster 3 model obtained an RMSE of 2.01°C and an adjusted $R^2$ value of 0.76. These metrics showed the model's robust performance and the ability to capture the complex thermal behavior of pavement systems with high accuracy. To evaluate the applicability of Equation 3 and the parameters presented in Table 8, model validation was performed against a test dataset. These figures showed the model's ability to accurately predict temperature profiles for datasets that were not included in the multivariable regression process.

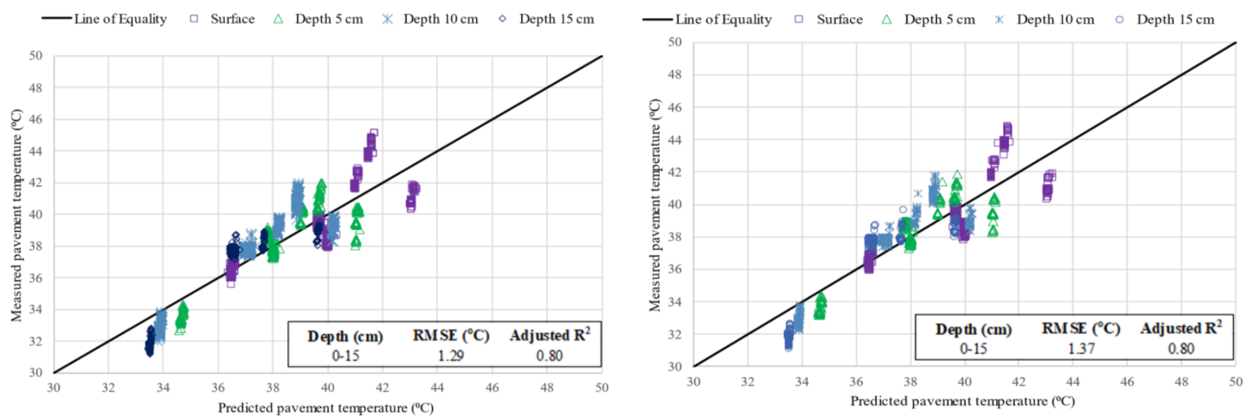


(a) (b)

**Figure 16. Maximum pavement temperature predictions at various depths compared to measured temperatures at Cluster 1 Airport; (a) Training Dataset, (b) Test Dataset**

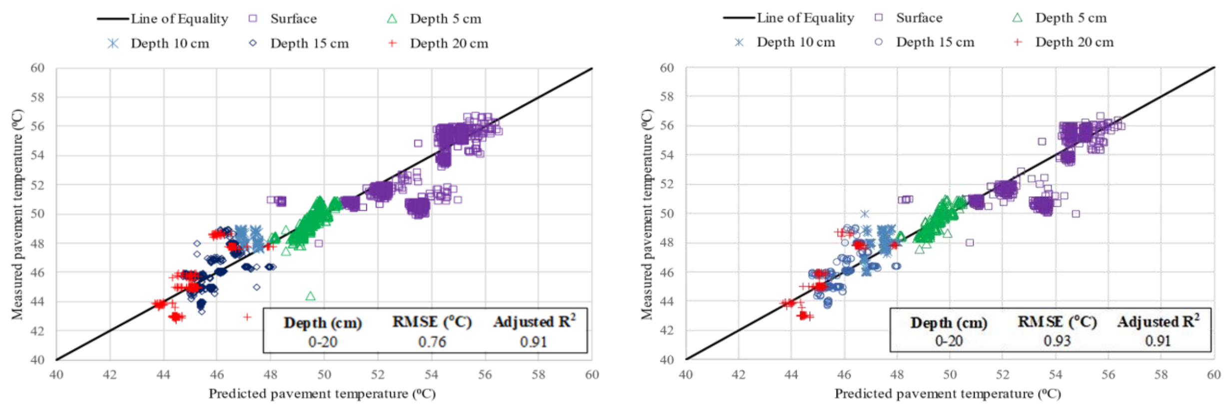


(a) (b)

**Figure 17. Maximum pavement temperature predictions at various depths compared to measured temperatures at Cluster 2 Airport; (a) Training Dataset, (b) Test Dataset**

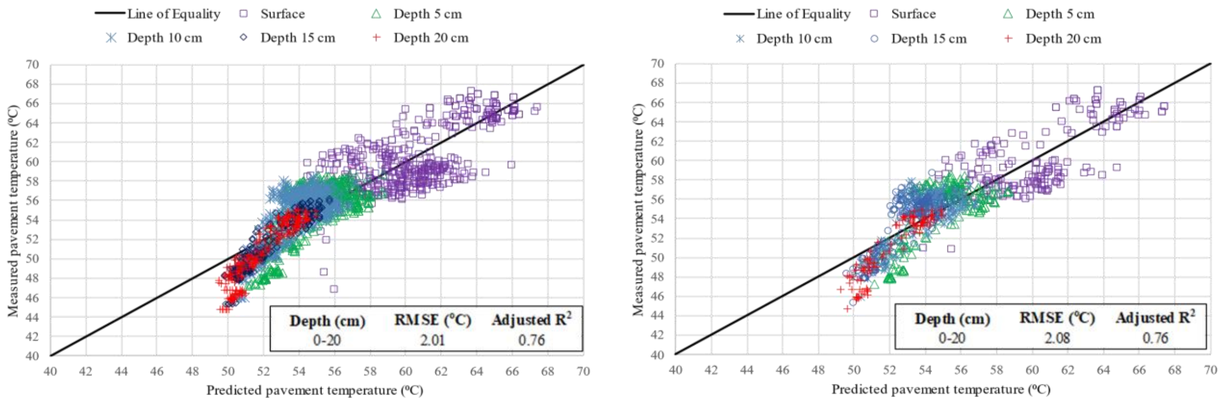


(a) (b)

**Figure 18. Maximum pavement temperature predictions at various depths compared to measured temperatures at Cluster 3; (a) Training Dataset, (b) Test Dataset**

An overview of the maximum temperature distribution patterns in asphalt pavement mixtures is provided in Figure 19. A comparative analysis was conducted by Ariawan et al. [28], which focused on a similar region in Cluster 3 Airport. The comparison showed significant improvements in predictive accuracy of the current model, as presented in Table 10.

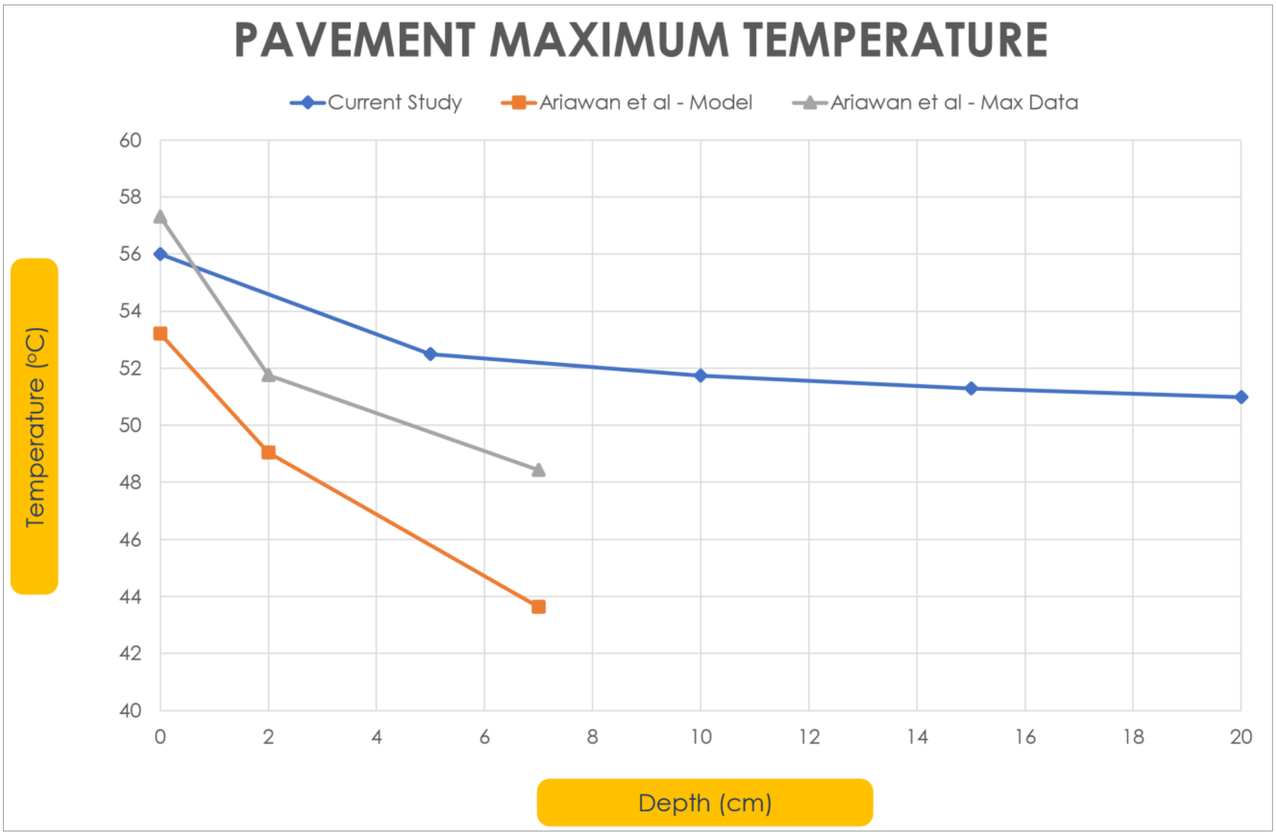


**Figure 19. Predicted temperature distribution for national road of Denpasar – Gilimanuk (Km 102)**

**Table 9. Climatic benchmarks for the maximum pavement temperature in national road of Denpasar – Gilimanuk**

| Aspect | Value |
|---|---|
| RH min (%) | 53.97 |
| $T_{air}$ max (ºC) | 31.85 |
| Elevation (m) | 20.73 |
| $T^{obs}_{pav,0}$ (ºC) | 57.31 |
| $T^{obs}_{pav,2}$ (ºC) | 51.75 |
| $T^{obs}_{pav,7}$ (ºC) | 48.44 |

Predictions using this model show improved results compared to the Ariawan et al. [28] study, which was based on maximum pavement temperature data collected from roads (Table 10). Moreover, the quality of pavement on roads might differ from airport pavements, as shown by the different temperature-to-depth gradient. This suggested the enhanced reliability and applicability of the new pavement maximum temperature model for Cluster 3 regions, characterized by hot tropical climates and low elevations. The comparison underscores the significant improvement caused by the predictive model over the previous report. This advancement not only enhances the understanding of temperature distributions in tropical pavements but also provides a reliable tool for performance-based design and maintenance of asphalt pavements in challenging climatic conditions.

**Table 10. Predicted pavement maximum temperature distribution**

| Previous Model [28] | | Current Model | |
|---|---|---|---|
| d (cm) | $T_{pav,d}^{max}$ (ºC) | d (cm) | $T_{pav,d}^{max}$ (ºC) |
| 0 | 53.21 | 0 | 55.99 |
| 2 | 49.04 | 5 | 52.49 |
| 7 | 43.63 | 10 | 51.74 |
| | | 15 | 51.30 |
| | | 20 | 50.98 |

## 12. Conclusions

In conclusion, this study presented a comprehensive framework for predicting pavement temperature distribution at Indonesian airports, emphasizing the critical influence of temperature on the performance and durability of flexible pavements. By using data from 13 airports spanning diverse climatic and geographical conditions, a robust predictive model was developed, a clustering framework to optimize pavement material selection and design.

A key innovation in this study was the use of AirPaSS, a device for real-time pavement temperature monitoring. AirPaSS used advanced thermocouple sensors embedded at various depths, powered by a solar-energy management system and integrated with automated data transmission. This ensured continuous and accurate data collection, including active airside regions. The AirPaSS-enhanced dataset significantly improved the predictive model's reliability, offering deeper insights into pavement thermal behavior across different airport environments. This system represented a major advancement in pavement monitoring technology with potential applications extending beyond the aviation sector.

Based on hierarchical clustering, airports were grouped into three distinct clusters based on air temperature, surface pavement temperature, and elevation. These clusters provide actionable insights into environmental factors affecting pavement performance, enabling material designs that addressed the specific thermal conditions of each group. Furthermore, the clustering framework supported more resilient and cost-effective pavement solutions for the Indonesian aviation industry.

A predictive model, incorporating air temperature, elevation, and pavement depth, was formulated using a mixed linear and logarithmic regression method. The results showed high predictive accuracy, with RMSE values between 0.91°C and 2.01°C and Adjusted $R^2$ ranging from 0.76 to 0.91. This validated the model's reliability and applicability under diverse environmental conditions. The inclusion of practical constraints ensures its adaptability across airports with varying climatic challenges.

The integration of the predictive model with the clustering framework provided a systematic and scalable solution for optimizing airport pavement design. By addressing environmental and climatic variations, this study promoted the adoption of performance-based grading systems, moving beyond traditional penetration-grade specifications. The results provide a strong foundation for enhancing airport infrastructure resilience in tropical regions, contributing to improved safety, longevity, and cost-efficiency. Moreover, future investigations should explore the application of the framework in other regions with similar climatic challenges to validate and refine the methods proposed in this study.

## 13. Declarations

### 13.1. Author Contributions

Conceptualization, P.H., A.S., B.S.S., and E.S.H.; methodology, P.H. and B.S.S.; formal analysis, P.H. and B.S.S.; investigation, P.H., A.S., B.S.S., and E.S.H.; resources, P.H. and B.S.S.; data curation, P.H., B.S.S., and E.S.H.; writing—original draft preparation, P.H. and B.S.S.; writing—review and editing, P.H., A.S., B.S.S., and E.S.H.; visualization, P.H. and E.S.H.; supervision, A.S., B.S.S., and E.S.H.; funding acquisition, P.H. and B.S.S. All authors have read and agreed to the published version of the manuscript.

### 13.2. Data Availability Statement

The data presented in this study are available on request from the corresponding author.

### 13.3. Funding

The authors received no financial support for the research, authorship, and/or publication of this article.

### 13.4. Conflicts of Interest

The authors declare no conflict of interest.

## 14. References

[1] Al-Suleiman, T. I., Basma, A. A., & Ksaibati, K. (1993). Examination of pure environmental effects on pavement condition. Transportation Research Record, 1388, 52–59.

[2] Sulejmani, P., Said, S., Agardh, S., & Ahmed, A. (2021). Impact of temperature and moisture on the tensile strain of asphalt concrete layers. International Journal of Pavement Engineering, 22(13), 1711–1719. doi:10.1080/10298436.2020.1715404.

[3] Ebrahim Abu El-Maaty, A. (2017). Temperature Change Implications for Flexible Pavement Performance and Life. International Journal of Transportation Engineering and Technology, 3(1), 11. doi:10.11648/j.ijtet.20170301.11.

[4] Losa, M., Bacci, R., & Leandri, P. (2008). A statistical model for prediction of critical strains in pavements from deflection measurements. Road Materials and Pavement Design, 9(Sup 1), 373–396. doi:10.1080/14680629.2008.9690175.

[5] Lukanen, E. O., Stubstad, R., Briggs, R. C., & Intertec, B. (2000). Temperature predictions and adjustment factors for asphalt pavement (No. FHWA-RD-98-085; DBNX94822-D; NTIS-PB2000107444). Turner-Fairbank Highway Research Center, McLean, United States.

[6] Marshall, C., Meier, R., & Welch, M. (2001). Seasonal temperature effects on flexible pavements in Tennessee. Transportation Research Record, 1764, 89–96. doi:10.3141/1764-10.

[7] Wibowo, A., Subagio, B. S., Rahman, H., & Frazila, and R. B. (2024). Evaluation of the Airport Pavement Condition Index in the Aircraft Lateral Wander Area. International Journal of GEOMATE, 27(122), 87–95. doi:10.21660/2024.122.g13151.

[8] Ntramah, S., Tutu, K. A., Tuffour, Y. A., Adams, C. A., & Adanu, E. K. (2023). Evaluation of Selected Empirical Models for Asphalt Pavement Temperature Prediction in a Tropical Climate: The Case of Ghana. Sustainability, 15(22), 15846. doi:10.3390/su152215846.

[9] Direktorat Jenderal Bina Marga. (2024). Road Pavement Design Manual. No. 03/M/BM/2024. Direktorat Jenderal Bina Marga, Jakarta, Indonesia. (In Indonesian).

[10] Akbulut, H., Atilgan Gevrek, L., & Ay, M. (2024). Modeling of Asphalt Pavement Surface Temperature for Prevention of Icing on the Surface. Turkish Journal of Civil Engineering, 35(2), 1–21. doi:10.18400/tjce.1211542.

[11] Herry, P., Subagio, B. S., Hariyadi, E. S., & Wibowo, S. S. (2024). Integrating Regional Pavement Temperature into Simplified Material Characterization for Airport Pavement Rating. International Journal of GEOMATE, 27(120), 85–95. doi:10.21660/2024.120.g13162.

[12] Sun, L. (2016). Structural Behavior of Asphalt Pavements. Butterworth-Heinemann, Oxford, United Kingdom. doi:10.1016/C2014-0-02643-3.

[13] Adwan, I., Milad, A., Memon, Z. A., Widyatmoko, I., Ahmat Zanuri, N., Memon, N. A., & Yusoff, N. I. M. (2021). Asphalt Pavement Temperature Prediction Models: A Review. Applied Sciences, 11(9), 3794. doi:10.3390/app11093794.

[14] Zhang, J., Fwa, T. F., Tan, K. H., & Shi, X. P. (2003). Model for nonlinear thermal effect on pavement warping stresses. Journal of Transportation Engineering, 129(6), 695–702. doi:10.1061/(ASCE)0733-947X(2003)129:6(695).

[15] Asefzadeh, A., Hashemian, L., & Bayat, A. (2017). Development of statistical temperature prediction models for a test road in Edmonton, Alberta, Canada. International Journal of Pavement Research and Technology, 10(5), 369–382. doi:10.1016/j.ijprt.2017.05.004.

[16] Alavi, M. Z., Pouranian, M. R., & Hajj, E. Y. (2014). Prediction of asphalt pavement temperature profile with finite control volume method. Transportation Research Record, 2456(1), 96–106. doi:10.3141/2456-10.

[17] Ayasrah, U. B., Tashman, L., AlOmari, A., & Asi, I. (2023). Development of a temperature prediction model for flexible pavement structures. Case Studies in Construction Materials, 18, e01697. doi:10.1016/j.cscm.2022.e01697.

[18] Huang, Y., Nojumi, M. M., Ansari, S., Hashemian, L., & Bayat, A. (2024). Multi-depth temperature prediction using machine learning for pavement sections. Journal of Applied Remote Sensing, 18(01), 4517. doi:10.1117/1.jrs.18.014517.

[19] Kebede, Y. B., Yang, M. Der, & Huang, C. W. (2024). Real-time pavement temperature prediction through ensemble machine learning. Engineering Applications of Artificial Intelligence, 135, 1–21. doi:10.1016/j.engappai.2024.108870.

[20] Diefenderfer, B. K., Al-Qadi, I. L., & Diefenderfer, S. D. (2006). Model to predict pavement temperature profile: Development and validation. Journal of Transportation Engineering, 132(2), 162–167. doi:10.1061/(ASCE)0733-947X(2006)132:2(162).

[21] Chao, J., & Jinxi, Z. (2018). Prediction Model for Asphalt Pavement Temperature in High-Temperature Season in Beijing. Advances in Civil Engineering, 2018, 1–11. doi:10.1155/2018/1837952.

[22] Hassan, H. F., Al-Nuaimi, A., Al-Oraimi, S., & Jafar, T. M. A. (2008). Development of asphalt binder performance grades for Omani climate. Construction and Building Materials, 22(8), 1684–1690. doi:10.1016/j.conbuildmat.2007.06.016.

[23] Zeiada, W., Ashour, A. G., Mirou, S. M., Abuzwidah, M., & Shanablah, A. (2024). Development of superpave asphalt binder specifications to meet climate conditions in the UAE. International Journal of Pavement Engineering, 25(1), 2386627. doi:10.1080/10298436.2024.2386627.

[24] Wahhab, H. I. A.-A., Asi, I. M., & Ramadhan, R. H. (2001). Modeling Resilient Modulus and Temperature Correction for Saudi Roads. Journal of Materials in Civil Engineering, 13(4), 298–305. doi:10.1061/(asce)0899-1561(2001)13:4(298).

[25] Tabatabaie, S. A., Ziari, H., & Khalili, M. (2008). Modeling Temperature and Resilient Modulus of Asphalt Pavements for Tropic Zones of Iran. Asian Journal of Scientific Research, 1(6), 579–588. doi:10.3923/ajsr.2008.579.588.

[26] Salem, H. A. (2015). Research of the relevant temperatures for the design of pavement constructions on the desert roads in Libya. Ph.D. Thesis, University of Novi Sad, Novi Sad, Serbia.

[27] Nivitha, M. R., & Krishnan, J. M. (2014). Development of Pavement Temperature Contours for India. Journal of the Institution of Engineers (India): Series A, 95(2), 83–90. doi:10.1007/s40030-014-0074-y.

[28] Ariawan, I. M. A., Subagio, B. S., & Setiadji, B. H. (2015). Development of asphalt pavement temperature model for tropical climate conditions in West Bali region. Procedia Engineering, 125, 474–480. doi:10.1016/j.proeng.2015.11.126.

[29] Ntramah, S., Tutu, K. A., & Tuffour, Y. A. (2024). Development of Asphalt Pavement Temperature Prediction Models for Sub-Saharan Tropical Climate: The Case of Ghana. International Journal of Pavement Research and Technology. doi:10.1007/s42947-024-00451-x.

[30] Herry, P., Subagio, B. S., Susanto, E. H., & Wibowo, S. S. (2024). Development of Maximum Temperature Prediction Model within Asphalt Pavement Layers for Airports in Tropical Regions. 18th East Asia-Pacific Conference on Structural Engineering and Construction (EASEC-18), 13-15 November, 2024, Chiang Mai, Thailand.

[31] Shrivastav, A. (2021). Research Paper for Smart Home Automation System using ESP32 with Blynk, IR Remote & Manual control Relay, IoT Project. International Journal of Innovative Research in Electrical, Electronics, Instrumentation and Control Engineering, 9(5), 368–372.

[32] M. Broell, L., Hanshans, C., & Kimmerle, D. (2023). IoT on an ESP32: Optimization Methods Regarding Battery Life and Write Speed to an SD-Card. Edge Computing - Technology, Management and Integration. IntechOpen, London, United Kingdom. doi:10.5772/intechopen.110752.

[33] Christopher, J. O., Resquites, M., Parrocho, M. A., Vinegas, N., Vinyl, D. R., & Oquiño, H. (2023). IoT-Based Temperature Monitoring and Automatic Fan Control Using ESP32. IRE Journals, 7(5), 35–44.

[34] Kengkla, N., Ratanaphan, S., Earmyang, T., Chokdurong, M., & Tisa, P. (2020). The rejuvenation of valve-regulated lead-acid (VRLA) battery with pulse width modulation (PWM) charging and ultrasonic (No. 2775). EasyChair, Wythenshawe, United Kingdom.

[35] Tang, J.-X., Du, J.-H., Lin, Y., & Jia, Q.-S. (2020). Predictive Maintenance of VRLA Batteries in UPS towards Reliable Data Centers. IFAC-PapersOnLine, 53(2), 13607–13612. doi:10.1016/j.ifacol.2020.12.854.

[36] de Anda, M. F., Butler, P. C., Miller, J. L., & Moseley, P. T. (2004). Reliability of valve-regulated lead-acid batteries for stationary applications (No. SAND2004-0914). Sandia National Laboratories (SNL), Albuquerque, United States.

[37] Kong, H., Wang, J., Cai, L., Cao, J., Zhou, M., & Fan, Y. (2024). Surface Solar Radiation Resource Evaluation of Xizang Region Based on Station Observation and High-Resolution Satellite Dataset. Remote Sensing, 16(8), 1405. doi:10.3390/rs16081405.

[38] Huang, Y. H. (2004) Pavement Analysis and Design (2nd Edition). Pearson Prentice Hall, Upper Saddle River, United States.

[39] RDO Asphalt 09/24. (2009). Guidelines for the calculation of the superstructure of traffic areas with asphalt surface layer. FGSV Verlag, Köln, Germany. (In German).

[40] Kleizienė, R., Vaitkus, A., Židanavičiūtė, J., & Marcinkevičius, E. (2017). Classification of surface temperature for the flexible pavement design. Proccedings of 10th International Conference "Environmental Engineering." doi:10.3846/enviro.2017.139.

[41] Lasdon, L. S., Fox, R. L., & Ratner, M. W. (1974). Nonlinear optimization using the generalized reduced gradient method. Revue Française d'automatique, Informatique, Recherche Opérationnelle. Recherche Opérationnelle, 8(V3), 73–103. doi:10.1051/ro/197408v300731.